ELSEVIER

Journal of Structural Geology 27 (2005) 2150–2158

JOURNAL OF STRUCTURAL GEOLOGY

www.elsevier.com/locate/jsg

Regional stress field as determined from electromagnetic radiation in a tunnel

Marco Lichtenberger*

Geologisch-Paläontologisches Institut, Ruprecht-Karls-Universität Heidelberg, Im Neuenheimer Feld 234, 69120 Heidelberg, Germany

Received 22 February 2005; received in revised form 8 July 2005; accepted 2 August 2005
Available online 13 September 2005

Abstract

The paper presents the results of electromagnetic radiation (EMR) measurements in the Feuerberg tunnel in southwest Germany. EMR is associated with small scale fracturing processes. The measured numbers of EMR impulses are shown to be proportional to shear stresses. From the correlation of EMR and shear stresses along the long axis of the tunnel, orientations and magnitudes of the horizontal principal stresses are determined. The major horizontal principal stress is 3.6 ± 0.3 MPa and has an azimuth of $143 \pm 6°$. The minor principal horizontal stress is 2.1 ± 0.3 MPa. Zones in the tunnel are located where low shear stresses occur because vertical overburden and horizontal stresses are equal. In these zones also minimum radiation was detected. A possible stress accumulation close to a fault is suggested by higher EMR values in a part of the tunnel. Orientations and magnitudes of the horizontal principal stresses, which are derived from the measurements of EMR, correlate well with conventional stress measurements. It is suggested that the cross-section measuring method described in the study is used to determine regional stress fields as well as to investigate endangered zones with high stresses in underground facilities, which may be critical with regard to stability.

Keywords: Electromagnetic radiation; Microcracks; Nanocracks; Stress field; Tunnel; Shear stress

1. Introduction

Numerous investigations show a relationship between applied stress and electromagnetic radiation (EMR) emitted from rock material (e.g. Hadjicontis and Mavromatou, 1994; Krylov and Nikiforova, 1996; Reuther et al., 2002). Results from modelling (e.g. Molchanov and Hayakawa, 1995; O'Keefe and Thiel, 1995; Mognaschi, 2002), laboratory experiments (e.g. Cress et al., 1987; Frid et al., 1999, 2005; Koktavy et al., 2004) as well as field measurements (Frid, 1997, 2001; Lichtenberger, submitted for publication) suggest that small scale fracturing processes are the source of this EMR. Several atomic scale models based on the oscillation of dipoles at crack walls or crack tips (e.g. Gershenzon et al., 1987; Mognaschi, 2002) have been proposed. Recently, it has been suggested that EMR may be emitted by surface vibrational optical waves due to the breaking of atomic bonds during crack propagation (Bahat et al., 2005). EMR emission may start as early as in the nucleation phase of nanocracks (cracks $< 10^{-6}$ m) during crystal deformation and accompanying polarization along the future nanocracks (Teisseyre, 1992). Since nanocracks and microcracks are sources of EMR, it should be possible to determine loci of high shear stress and tensional stress by measuring the EMR a long time before any macroscopic failure may occur (Frid, 1997, 2001).

Earlier work has shown that it is possible to determine parameters of the regional stress field such as the principal directions of stress from measurements of EMR at the earth's surface (Lichtenberger, submitted for publication). The purpose of this investigation is to show how the regional stress field may be analyzed and quantified from measurements of EMR in a tunnel using well established rock mechanics in combination with new measuring methods.

2. Geological background

2.1. Regional geology

The measurements discussed in this paper were undertaken in the early Mesozoic rocks of central Europe, to the east of the Upper Rhine Graben. These rocks are

* Tel.: +49 6221 54 43 86.
E-mail address: mlichten@ix.urz.uni-heidelberg.de.

0191-8141/$ - see front matter © 2005 Elsevier Ltd. All rights reserved.
doi:10.1016/j.jsg.2005.08.002

exposed in the Feuerberg tunnel between Hirschhorn und Eberbach in southwest Germany (Fig. 1). The tunnel is located in the Rotenberg Anticline, which is part of the Hirschhorn Buntsandstein block (lower Triassic continental red beds). This block is bordered by the Finsterbach fault zone in the West and the Allemühl fault zone in the East. The tunnel traverses the so-called pseudomorph sandstone member of the middle Buntsandstein formation (Lower Triassic). The rock consists of red, fine- to coarse-grained sandstone. The upper part of the member features several red shale layers (Hasemann, 1928).

Two faults of the Hirschhorn Buntsandstein block are located in the vicinity of the tunnel (Fig. 1). Their position, as shown in Fig. 1, was suggested by the mapping geologist; their exact position is unknown (Hasemann, 1928). One fault is located NW of the tunnel; the other fault is supposed to cut the tunnel at its eastern end. Both faults are striking approximately N–S. Similarly oriented faults from the same region are of upper Eocene to Miocene age with a maximum activity in Pliocene times (Becksmann, 1975).

The Feuerberg tunnel has a length of 966 m and is about 150 m above sea level. Its cross-section has a diameter of about 6.5 m (Fig. 1). It is used by the railway from Heidelberg to Neckarelz. The measurements started at the western end of the tunnel, so the position 0 m in longitudinal sections along the tunnel axis refers to this end in Figs. 3, 4, 6 and 7, respectively.

2.2. Regional stress field

The regional stress field of Southwest Germany is well known from focal plane solutions (Ahorner, 1975) and in situ measurements (Schmitt, 1981) and EMR measurements (Lichtenberger, submitted for publication). It is influenced by stresses from the Alpine orogen as well as from the Upper Rhine Graben (Baumann, 1982). All three methods revealed a median direction of the major horizontal principal stress σ_H of about $145 \pm 20°$ (Fig. 1). The in situ measurements showed that σ_H is 3.6 ± 1.6 MPa and the minor horizontal principal stress σ_h is 1.6 ± 0.8 MPa. The in situ measurements (overcoring method) closest to the Feuerberg tunnel have been undertaken in Auerbach (49°43′/08°39′) near the eastern border of the Upper Rhine Graben (Greiner, 1976). From these in situ measurements the direction of σ_H was determined as 125°; σ_H was calculated to be 3.3 MPa and σ_h is 2.1 MPa.

Earlier EMR measurements 20 km east of the Feuerberg tunnel suggest that σ_H has a median direction of 137° and the relation of principal horizontal stresses k_{horiz} ($=\sigma_H/\sigma_h$) is about 2.4 (Lichtenberger, submitted for publication).

3. Measuring method and results

EMR from fracturing processes occurs as pulsed radiation (Rabinovitch et al., 1996, 2000; Bahat et al., 2005). Most often several pulses occur together as an EMR burst. Due to these characteristics they can easily be separated from periodic anthropogenic radiations. A Cerescope was used as the measuring device for this investigation (Obermeyer, 2005). This is a portable device with a ferrite aerial. The EMR is detected and processed by a microprocessor-controlled receiver, A/D converter and digital logical circuitry. Pulse numbers and energy are

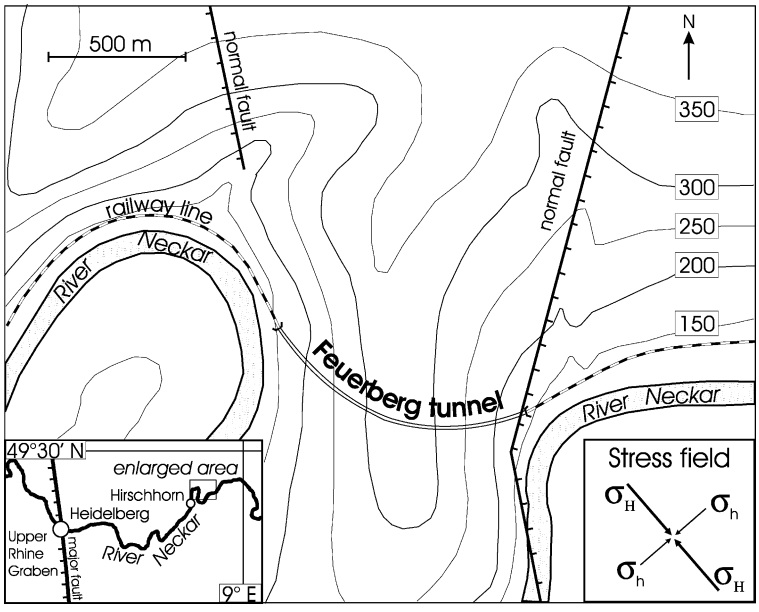

Fig. 1. Map showing the situation of the Feuerberg tunnel. Also illustrated are two assumed faults in the vicinity of the tunnel (for discussion see text). Topographic contours are in metres above sea level. Inset in the lower right corner shows orientation of the horizontal principal stresses derived from in situ measurements (see text for references). Inset map in the lower left corner shows regional situation of the tunnel to the east of the Upper Rhine Graben.

stored in the RAM and may be transferred to a PC using the RS232 interface. The Cerescope was developed by Ceres GmbH, Staffort (Germany). A frequency range of 30–50 kHz and an amplification of 102 dB were used during the measurements.

The measurements in the Feuerberg tunnel were carried out as 'cross-section measurements' (Fig. 2a) normal to the tunnel orientation: the aerial is directed vertically, towards the top of the tunnel, and a first measurement is taken. The next measurement is 5° away, along the cross-section etc., until a full circle of 360° is finished. A cross-section measurement consists therefore of 72 single measurements. Each single measurement documents the number of impulses detected in 100 ms; this number is abbreviated as the 'impulse number'. The single measurements are compiled into polar diagrams (Fig. 2b). The results are projected onto a cross-section of the tunnel (Fig. 2c); the maximum impulse numbers are shown. Seventy-one of these cross-sections have been measured along the longitudinal axis of the tunnel in irregular intervals based on the construction blocks of the tunnel. These cross-section measurements comprise 5112 single measurements. In addition, several cross-section measurements were repeated at selected points of the tunnel to verify the reproducibility of the measurements. They were well reproducible. All sections show maximum impulse numbers at angles of about 45, 135, 225 or 315° with the horizontal plane in the centre of tunnel cross-section. The maximum impulse numbers are illustrated in Fig. 3.

The measurements reveal several important features:

1. If EMR is of atmospheric origin the minimum impulse numbers should be located in the middle of the tunnel, where overburden is largest and atmospheric EMR would be filtered by the rock mass. The overburden in the middle of the tunnel is about 180 m (compare with Fig. 4 and topography in Fig. 1). Since the skin depth of EMR with a frequency of 30 kHz is about 30 m in comparable rocks, it is unlikely to measure any signal from the surface at a depth of 180 m with the applied measuring technique. The skin depth is calculated from EMR-frequency, electric resistivity and magnetic permeability of the rock. For more detail with regard to the skin depth of EMR see Mognaschi (2002) and Lichtenberger (submitted for publication). Therefore, it can be assumed that the EMR originates from the lithosphere.
2. In the context of surface measurements (Lichtenberger, submitted for publication) it was discussed if the aerial also might detect EMR from its rear end. If true, Fig. 2b and c should also contain maxima of impulse numbers at angles of 45 and 315°. However, the measurements described in this paper show that there is no such effect. It can be concluded that the aerial only detects EMR from the direction to where its tip is pointed. The symmetry effect of the aerial is irrelevant. Therefore, the measuring method is highly appropriate for direction finding techniques such as the one used in this investigation.
3. Two areas in the tunnel with a length each of approximately 80 m may be differentiated, since a minimum EMR was detected (Fig. 3). Between these

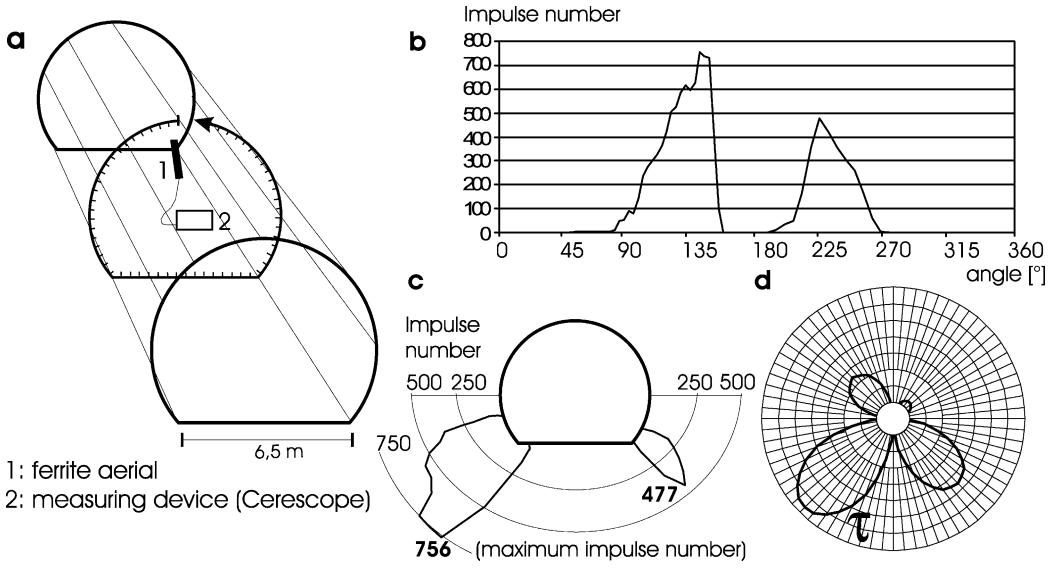

Fig. 2. Measurement and evaluation of cross-section measurements. (a) Orientation of the aerial during measurements in the tunnel. The first measurement is started with the aerial oriented vertically and pointed to the top of the tunnel. Then every 5° further measurements are taken around the tunnel section until the top of the tunnel is reached again. (b) Polar diagram showing results of a cross-section measurement from the Feuerberg tunnel. Maximum impulse numbers were measured at angles of 135 and 225° to the vertical. (c) The same EMR data projected onto the cross-section of the tunnel. (d) Shear stress calculated using the Kirsch-formula (Hudson and Harrison, 1997) and also illustrated in a polar diagram. The calculated shear stresses correlate well with the EMR measurements.

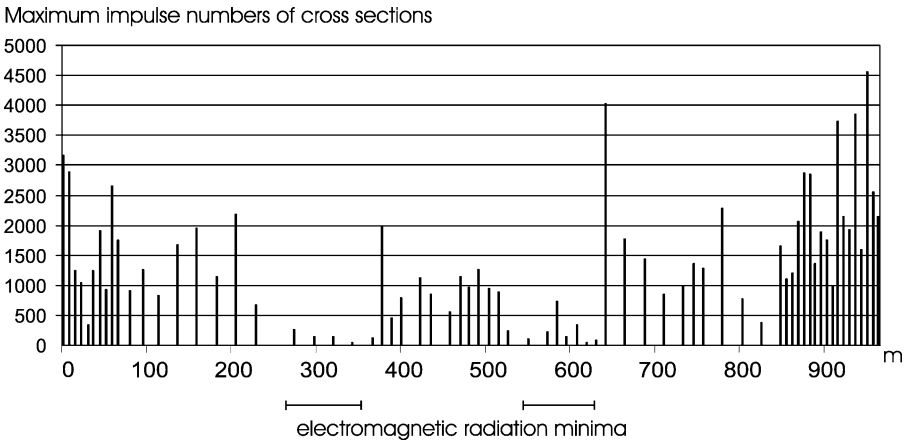

Fig. 3. Compilation of all cross-section measurements used in this study along the long axis of the tunnel. Maximum impulse numbers are shown. 0 m refers to the western end of the tunnel. The largest impulse numbers occur at the ends of the tunnel. Two zones of minimum EMR can be distinguished, while in the middle of the tunnel higher impulse numbers were measured.

two areas higher impulse numbers up to 1200 were measured. These measurements may indicate that there are zones in the tunnel where almost no nanocracks or microcracks exist, indicating minimum shear stress. This feature is discussed further below.

4. Discussion

This chapter describes how magnitude and orientation of the regional stress field may be derived from EMR measurements in combination with conventional rock mechanics. First, the stress field around the tunnel is calculated from overburden and rock density. Then the distributions of horizontal stresses and shear stresses along the longitudinal axis of the tunnel are described. These stresses cannot be quantified by rock mechanic methods only because magnitude and orientation of the regional stresses are unknown a priori. From the correlation of EMR values and possible shear stress distributions magnitude and orientation of the regional stresses are determined.

4.1. Stress field around the tunnel

The stress field at any point in the lithosphere is described by an ellipsoid with the axes of principal directions of stress σ_{1-3}. For our purposes the major horizontal principal stress is termed σ_H, the minor σ_h; and the remaining vertical principal stress is termed σ_V. Only compressive stresses are considered in this paper; no tensile stresses are reported in the investigated region (Baumann, 1982). The regional stress field around a tunnel, with regard to its cross-section, may be described by only two stresses: the vertical stress σ_V and the effective horizontal stress σ_{eff} normal to the tunnel long axis (Fig. 5).

These two stresses induce a secondary stress field around the tunnel due to the open space of the tunnel. This secondary stress field is defined by radial stress, tangential stress and shear stress τ, respectively (Hudson and Harrison, 1997). Most interesting with regard to this investigation are shear stresses, because these stresses may be the only ones leading to nanocracks and microcracks due to the absence of tensional stresses, where the overburden stress has a maximum of less than 4.5 MPa (Fig. 4) and a higher compressive strength of the sandstones is at least 15 MPa (Dachroth, 2002). At relatively small stresses, strain is proportional to stress (Hudson and Harrison, 1997). Therefore, it can be assumed that the number of microcracks and nanocracks and as a result the measured EMR impulse numbers, are proportional to shear stress. This proportionality is also shown by the cross-section measurements (Fig. 2) and, therefore, can be applied along the long axis of the tunnel.

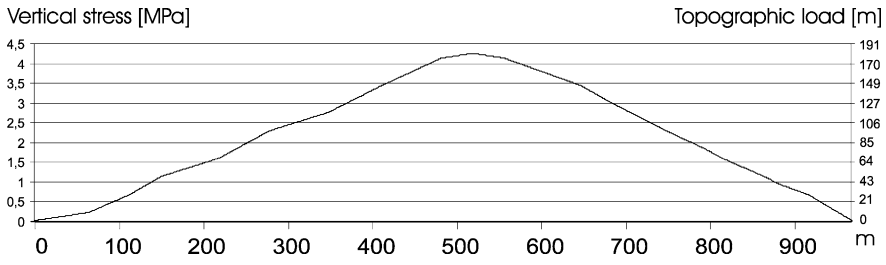

Fig. 4. Distribution of vertical stress σ_V along the longitudinal axis of the tunnel as calculated from topographic load and a median density of 2.35 t/m^3. 0 m refers to the western end of the tunnel.

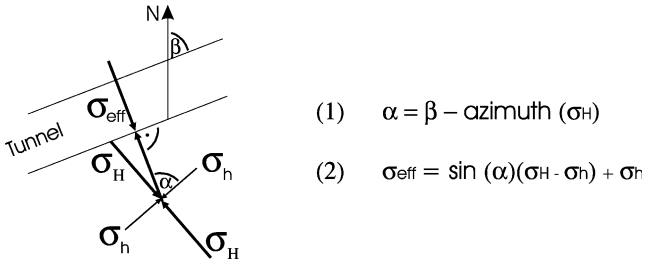

Fig. 5. Sketch for the calculation of effective horizontal stress σ_{eff} from the azimuth of the tunnel (β), azimuth of the major horizontal principal stress σ_H, and the horizontal principal stresses σ_H and σ_h.

In order to investigate shear stresses, the vertical stress σ_V and the effective horizontal stress σ_{eff} along the longitudinal axis of the tunnel are described. From σ_V and σ_{eff} shear stresses are calculated using the standard equations (Hudson and Harrison, 1997). Because of the relatively simple geological conditions, both horizontal and overburden stresses can be reliably calculated.

Vertical stress σ_V can simply be calculated from the weight of the rock material on top of the tunnel along the longitudinal axis of the tunnel. Assuming an average density of 2.35 t/m^3 (Dachroth, 2002) (Fig. 4), the vertical stress does not exceed 4.5 MPa.

σ_{eff} is derived from three unknown quantities: σ_H, σ_h and the azimuth of σ_H (Fig. 5; Eqs. (1) and (2)). It can only be calculated if these three parameters are known. σ_{eff} is at a minimum when the longitudinal axis of a tunnel is normal to σ_h and parallel to σ_H. In this case, σ_{eff} equals σ_h. Maximum values of horizontal stress occur if a tunnel is perpendicular to σ_H. Since the three parameters are not known a priori, an unlimited number of horizontal stress distributions along the longitudinal axis of the tunnel are possible. Two examples of such possible distributions, based on different values of the three critical parameters, are given in Fig. 6.

From any possible distribution of horizontal stress σ_{eff} and the known value of vertical stress σ_V it is possible to calculate shear stress using the Kirsch-formula (Hudson and Harrison, 1997):

$$\tau = |(1/2)\sigma_V(1-(\sigma_{eff}/\sigma_V))(1+2(a^2/r^2) - 3(a^4/r^4))\sin(2\theta)| \quad (3)$$

where a = radius of the tunnel section (3.25 m); r = distance from the centre of the tunnel to the point behind the masonry for which shear stress is calculated = a + 0.5 m = 3.75 m; θ = angle from the horizontal plane in the centre of the tunnel section to the point for which shear stress is calculated.

Since maximum shear stresses are considered, θ may be 45, 135, 225 or 315°, because $|\sin(2\theta)|$ reaches its maximum for these respective angles (Fig. 2d). These angles also coincide with the directions at which maximum impulse numbers were measured (Fig. 2b and c). This correlation is explored further in a present study at the University of Heidelberg with regard to determining zones in underground facilities where failure or rockburst may occur.

Similar to the distributions of horizontal stress σ_{eff}, the distributions of shear stress τ are also dependent on σ_H, σ_h and the azimuth of σ_H. All other parameters of the Kirsch-formula for shear stress determination are known. As a consequence, an unlimited number of possible shear stress distributions exist. Although they are very sensitive to even small changes of the three critical parameters, the calculated shear stresses have two characteristics:

1. The highest shear stresses always occur at angles of 45, 135, 225 or 315° to a horizontal plane in the centre of the tunnel cross-section. Fig. 2d shows calculated shear stresses of a specific cross-section, which correlate well with the measured EMR (Fig. 2c).
2. The shear stresses increase towards the entrances of the tunnel. This is an effect of a decrease in topographic load towards the end of the tunnel, which results in $\sigma_{eff} \gg \sigma_V$.

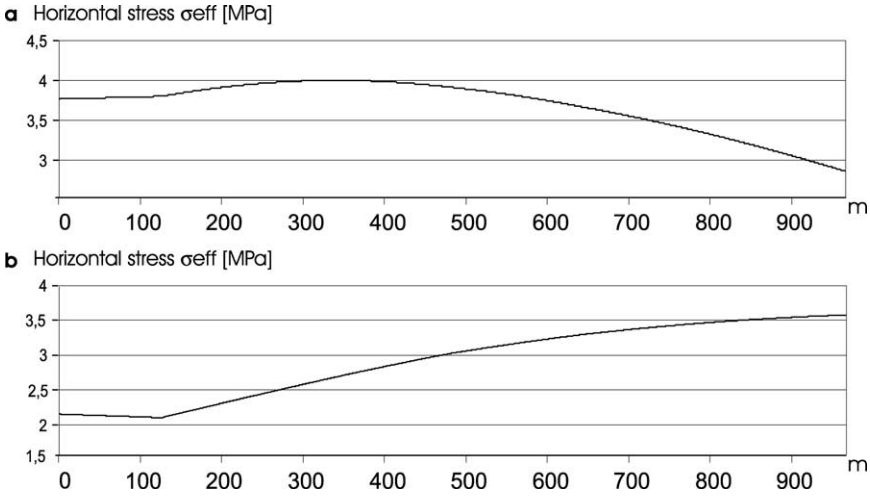

Fig. 6. Two examples of possible distributions of σ_{eff} calculated for different parameters. (a) σ_H = 4 MPa; σ_h = 1.5 MPa and azimuth (σ_H) = 30°. (b) σ_H = 3.6 MPa; σ_h = 2.2 MPa and azimuth (σ_H) = 143°. 0 m refers to the western end of the tunnel.

Such a relationship is also clear from the EMR-measurements (Fig. 3).

Many of the possible shear stress distributions show two points in the tunnel, where no shear stress occurs (Fig. 7). At these points vertical stress σ_V and horizontal stress σ_{eff} are equal. Between these two points shear stress is higher, since horizontal stress σ_{eff} is smaller than the vertical stress σ_V. The feature of two minima along the longitudinal section of the tunnel was also recognized in the EMR measurements above (Fig. 4).

At the entrances of the tunnel $\sigma_H = \sigma_1$, $\sigma_h = \sigma_2$ and $\sigma_V = \sigma_3$. Towards the middle of the tunnel $\sigma_V = \sigma_2$ and $\sigma_h = \sigma_3$. In the centre of the tunnel $\sigma_V = \sigma_1$, $\sigma_H = \sigma_2$ and $\sigma_h = \sigma_3$.

EMR origins from nano- and microfracturing (see Section 1) and fracturing processes around the Feuerberg tunnel are most probable in regions with high shear stresses (see above). As a consequence, a correlation of EMR and shear stresses is expected.

4.2. Correlation of EMR-measurements and stress calculations

A Microsoft Excel worksheet was developed in order to compare the different possible shear stress distributions with the EMR measurements along the tunnel axis (Fig. 3). Fig. 7 shows a best fitting graph for the parameters: $\sigma_H = 3.6 \pm 0.3$ MPa, $\sigma_h = 2.1 \pm 0.3$ MPa and an azimuth of $\sigma_H = 143 \pm 6°$. The deviations are given for graphs that show about 5% less fit with the measurements than the best fitting solution. From these values the relation of the two horizontal principal stresses $k_{horiz} = 1.7 \pm 0.4$ was calculated.

The values are consistent with in situ measurements discussed above (see Section 4.1) and fit well into the current ideas of the regional stress field. The values are also consistent with the results of former EMR measurements on the earth's surface that were undertaken in Lower Muschelkalk rocks (Middle Triassic marls, dolomites and limestones) about 20 km east of the Feuerberg tunnel (Lichtenberger, submitted for publication). The major difference from the results in the Feuerberg tunnel is the higher k_{horiz} in the Lower Muschelkalk area. It is hard to tell so far if this is a lithological effect, since k_{horiz} is also connected to the Poisson-ratio μ by $k_{horiz} = (1-\mu)/\mu$ in stress fields without further horizontal influence. It may also be possible that the decrease of k_{horiz} is a result of a further horizontal influence on the regional stress field, e.g. mantle currents below the Upper Rhine Graben structure, which were discussed by Strobach (1974).

Although EMR measurements and shear stress calculations show a general fit with each other (Fig. 7), a single zone in the tunnel shows significant deviation. The zone from 640 to 700 m shows extraordinary high impulse numbers. Their maximum is at 640 m and the measurements decrease abruptly towards the interior of the tunnel. They also decrease gradually to the eastern end. A possible explanation may be provided by stress accumulation along a fault, which may cut the tunnel at 640 m. The geological map shows an assumed fault close to the eastern end of the tunnel (Hasemann, 1928). Since its exact position could not be determined, it is perfectly possible that the exceptionally high EMR values indicate the location of this fault.

Another interesting aspect of the correlation of shear stresses and EMR is that it might be possible to gauge absolute stress values. Assuming the best fitting graph (Fig. 7) represents the actual shear stress distribution along the Feuerberg tunnel, 1 MPa corresponds to 2100 EMR pulses. This correlation is, of course, only valid for the specific parameters of the measurements (100 ms, 30–50 kHz, 102 dB amplification, maximum impulse numbers of cross-section measurement along tunnel long axis) as well as for the particular lithology. It is improbable that this factor represents a value that is generally valid.

In addition to the cross-section EMR measurements discussed above, several horizontal EMR measurements have been undertaken in and around the Feuerberg tunnel to determine the major horizontal principal direction of stress. For a detailed description of this method see Lichtenberger

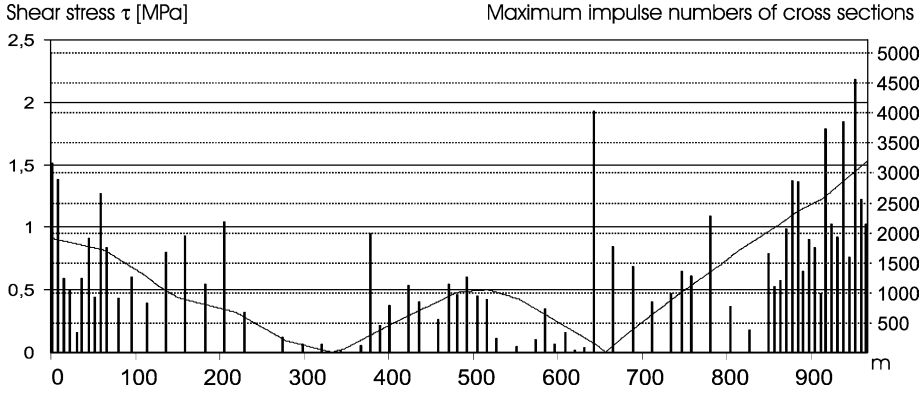

Fig. 7. Correlation of the best fitting distribution of shear stress τ with the EMR measurements (Fig. 3) along the longitudinal axis of the tunnel. Shear stress was calculated using the Kirsch-formula (Hudson and Harrison, 1997), vertical stress σ_V (Fig. 4) and σ_{eff} (Fig. 6b). There is a positive correlation except for the zone 640–700 m, which may be evidence for the local influence of a fault (compare Fig. 1). A shear stress of 1 MPa can be correlated with 2100 pulses.

(submitted for publication). Using the results from horizontal EMR measurements, the following parameters were determined: $\sigma_H = 141 \pm 9°$; $k_{horiz} = 2.1$. These values are consistent with the results obtained by cross-section measurements as well as with results from in situ techniques and focal plane solutions (Baumann, 1982).

The method of cross-section measurements and comparison with possible shear stress distribution graphs has the potential to be used to determine regional stress fields. The existence of zones with no shear stress and no EMR emission proved to be most valuable during the comparison process of measurements and possible shear stress distributions. If such zones did not occur, it would be difficult to find the best fitting graph for magnitudes and orientations of stresses with low deviations from the regional stress field.

As a consequence, it is recommended to use this method in tunnels where vertical stress and effective horizontal stress may be equal at one or more points of the longitudinal section of the tunnel. The more of these points that exist, the easier it will be to find a best fitting distribution of shear stresses and the more precise the parameters of the regional stress field can be determined. So far it is only known that this method may be used in compressive stress fields; its use in stress fields with tensile horizontal stress(es) has yet to be verified.

4.3. Discussion of other explanations

Although it could be shown here that EMR is associated with microfracturing processes, other geophysical phenomena were used to explain EMR emission. Therefore, it is briefly discussed why other processes can be excluded as EMR sources in the Feuerberg tunnel.

Numerous investigations have come to the conclusion that the movement of fluids in the lithosphere is the source of EMR (Mizutani et al., 1976; Fitterman, 1979; Ishido and Mizutani, 1981; Draganov et al., 1991). This effect is usually referred to as the 'electrokinetic effect'. Model calculations (Fenoglio et al., 1995) show that this effect may take place in joints of about 150 mm length to produce radiation of tens of kHz. No correlation of the orientation of such joints in the Lower Muschelkalk and the Buntsandstein with EMR was found (compare Lichtenberger, submitted for publication). Therefore it is difficult to explain the described measurements with this effect.

EMR was also interpreted as being of atmospheric or ionospheric origin (Nikiforova and Yadakhin, 1989). Earlier investigations (Morgunov and Matveyev, 1991; Gershenzon and Gokhberg, 1993) as well as our own data (see Section 3) show EMR to originate from within the lithosphere.

Mikhailenko and Soboleva (1997) and Molchanov et al. (2001) among others suggested an origin of EMR by movement of conductive material in the earth's magnetic field. Several studies showed this effect to be very weak (Gershenzon and Bambakidis, 2001) and unable to explain any of the EMR laboratory results (Nitsan, 1977).

Further, piezoelectric (Bishop, 1981) and piezomagnetic (Breiner and Kovach, 1968; Nagata, 1972; Carmichael, 1977) effects were considered to explain EMR. Another possible mechanism is the movement or deformation of charged crystal dislocations (Slifkin, 1993) and the movement of 'electric point defects' (= 'Elektronenstörstellen') (Kleber et al., 1990) or 'positive hole' charge carriers (Freund, 2000, 2003).

It is hard to see how these effects could explain the described measurements, since highest EMR values are expected to be spatially related with the highest local stresses and not shear stresses. If such effects were the source of EMR, maximum impulse numbers would be measured in zones with the highest general stresses. Tangential and radial stresses are much higher than shear stresses (Hudson and Harrison, 1997). Accordingly, the highest EMR measurements would be expected at angles of 0 or 90° to a horizontal plane in the centre of the tunnel cross-section. Some of the effects stated above may, however, contribute to EMR in general. There is some evidence that piezoelectricity may increase dipole moments during the stress release when microfractures open and therefore increase the EMR amplitudes (Nitsan, 1977; Cress et al., 1987).

The interpretation of EMR measurements in the Feuerberg tunnel as related to micro- and nanofracturing processes is plausible. It is consistent with well-known rock mechanics as well as with latest modelling and laboratory results on EMR (see Section 1) in general. In addition, the results obtained using this method are consistent with standard methods of stress determination such as the doorstopper method and the calculation of focal plane solutions (Baumann, 1982).

5. Conclusions

The results and discussions presented above lead to the following conclusions:

1. Micro- and nanofracturing processes are the source of EMR detected in the tunnel. Such processes occur preferably in zones, which feature high shear stresses; they are absent in zones with low or no shear stresses. No other sources of EMR have been detected.
2. The applied method may be an effective way to determine parameters of the regional stress field without influencing or even touching the rocks measured.
3. The method may also provide the possibility of determining zones in underground facilities that are endangered by any kind of rock failure, e.g. faults.
4. From the EMR data the regional stress field around the Feuerberg tunnel can be determined: the major principal horizontal stress $\sigma_H = 3.6 \pm 0.3$ MPa, its azimuth is $143 \pm 6°$. $\sigma_h = 2.1 \pm 0.3$ MPa. These values are obtained by correlation of EMR and calculated stresses. They are

consistent with results from conventional methods known from literature.

Acknowledgements

I thank Dr Obermeyer (Gesellschaft für Erkundung und Ortung, Karlsruhe). He generously provided a Cerescope as well as many valuable discussions and permanent support of the project and his constructive review. Prof. Dr Greiling (Geologisch-Paläontologisches Institut der Universität Heidelberg) provided valuable suggestions, comments and extensive help in the preparation of the manuscript. Messrs. Gilsdorf and Bauer (Deutsche Bahn Netz AG Südwest) permitted the measurements in the Feuerberg tunnel and the publication of the data. I thank Messrs. S. Traxel (UGI) and J. Zolk (GPI) for numerous helpful comments and Mrs N. Droste for her assistance in taking the measurements. I also acknowledge Dr Frid for the helpful review of the manuscript. This project is being funded by the Landesgraduiertenförderung of the University of Heidelberg.

References

Ahorner, L., 1975. Present-day stress field and seismotectonic block movements along major fault zones in Central Europe. Tectonophysics 29, 233–249.

Bahat, D., Rabinovitch, A., Frid, V., 2005. Tensile Fracturing in Rocks—Tectonofractographic and Electromagnetic Radiation Methods. Springer, Heidelberg.

Baumann, H., 1982. Spannung und Spannungsumwandlung im Rheinischen Schiefergebirge. Numismatischer Verlag, Koblenz.

Becksmann, E., 1975. Tektonik des Deckgebirges im Odenwald. Aufschluß Sonderheft 27, 281–283.

Bishop, J.R., 1981. Piezoelectric effects in quartz-rich rocks. Tectonophysics 77, 297–321.

Breiner, S., Kovach, R.L., 1968. Local magnetic events associated with displacement along the San Andreas Fault (California). Tectonophysics 6, 69–73.

Carmichael, R.S., 1977. Depth calculation of piezomagnetic effect for earthquake prediction. Earth and Planetary Sciences Letters 36, 309–316.

Cress, G., Brady, B., Rowell, G., 1987. Sources of electromagnetic radiation from fracture of rock samples in laboratory. Geophysical Research Letters 14 (4), 331–334.

Dachroth, W., 2002. Handbuch der Baugeologie und Geotechnik. Springer, Heidelberg.

Draganov, A.B., Inan, U.S., Taranenko, Y.N., 1991. ULF magnetic signatures at the earth surface due to ground water flow: a possible precursor to earthquakes. Geophysical Research Letters 18 (6), 1127–1130.

Fenoglio, M.A., Johnston, M.J.S., Byerlee, J.D., 1995. Magnetic and electric fields associated with changes in high pore pressure in fault zones; application to Loma Prieta ULF emissions. Journal of Geophysical Research 100, 12951–12958.

Fitterman, D.V., 1979. Theory of electrokinetic–magnetic anomalies in a faulted half-space. Journal of Geophysical Research 84 (B12), 6031–6040.

Freund, F.T., 2000. Time-resolved study of charge generation and propagation in igneous rocks. Journal of Geophysical Research 105 (B5), 11001–11020.

Freund, F.T., 2003. Rocks that crackle and sparkle and glow—strange pre-earthquake phenomena. Journal of Scientific Exploration 17(1), 37–71.

Frid, V., 1997. Electromagnetic radiation method for rock and gas outburst forecast. Journal of Applied Geophysics 38, 97–104.

Frid, V., 2001. Calculation of electromagnetic radiation criterion for rockburst hazard forecast in coal mines. Pure and Applied Geophysics 158, 931–944.

Frid, V., Rabinovitch, A., Bahat, D., 1999. Electromagnetic radiation associated with induced triaxial fracture in granite. Philosophical Magazine Letters 79, 79–84.

Frid, V., Bahat, D., Rabinovitch, A., 2005. Analysis of en échelon/hackle fringes and longitudinal splits in twist failed glass samples by means of fractography and electromagnetic radiation. Journal of Structural Geology 27, 145–159.

Gershenzon, N.I., Bambakidis, G., 2001. Modeling of seismo-electromagnetic phenomena. Russian Journal of Earth Sciences 3/4, 247–275.

Gershenzon, N.I., Gokhberg, M., 1993. On the origin of electrotelluric disturbances prior to an earthquake in Kalamata, Greece. Tectonophysics 224, 169–174.

Gershenzon, N.I., Gokhberg, M.B., Morgunov, V.A., Nikolaevskiy, V.N., 1987. Sources of electromagnetic emissions preceding seismic events. Izvestiya Akademii Nauk SSSR—Physics of the Solid Earth 23 (2), 96–101.

Greiner, G., 1976. In situ Spannungsmessungen und tektonischer Beanspruchungsplan in Südwestdeutschland. Geologische Rundschau 65, 55–65.

Hadjicontis, V., Mavromatou, C., 1994. Transient electric signals prior to rock failure under uniaxial stress. Geophysical Research Letters 21, 1687–1690.

Hasemann, W., 1928. Erläuterungen zu Blatt Eberbach (Nr. 24) der geologischen Spezialkarte von Baden. Herder, Freiburg.

Hudson, J.A., Harrison, J.P., 1997. Engineering Rock Mechanics—An Introduction to the Principles. Pergamon, Oxford.

Ishido, T., Mizutani, H., 1981. Experimental and theoretical basis of electrokinetic phenomena in rock–water systems and its applications to geophysics. Journal of Geophysical Research 86, 1763–1775.

Kleber, I., Bautsch, H.-J., Bohm, J., 1990. Einführung in die Kristallographie. Technik, Berlin.

Koktavy, P., Pavelka, J., Sikula, J., 2004. Characterization of acoustic and electromagnetic emission sources. Measurement Science and Technology 15, 973–977.

Krylov, S.M., Nikiforova, N.N., 1996. On ultralow frequency electromagnetic emission from an active geological medium. Physics of the Solid Earth 31 (6), 499–512.

Lichtenberger, M., 2005. Determination of horizontal principal directions of stress in the Lower Muschelkalk in Northern Baden-Württemberg (Germany) from geogenic electromagnetic radiations. Neues Jahrbuch für Geologie und Paläontologie—Abhandlungen, in press.

Mikhailenko, B.G., Soboleva, O.N., 1997. Mathematical modeling of seismomagnetic effects arising in the seismic wave motion in the earth's constant magnetic field. Applied Mathematics Letters 10 (3), 47–51.

Mizutani, H., Ishido, T., Yokokura, T., Ohnishi, S., 1976. Electrokinetic phenomena associated with earthquakes. Geophysical Research Letters 3, 365–368.

Mognaschi, E.R., 2002. On the possible origin, propagation and detectability of electromagnetic precursors of earthquakes. Atti Ticinensi di Scienze della Terra 43, 111–118.

Molchanov, O.A., Hayakawa, M., 1995. Generation of ULF electromagnetic emissions by microfracturing. Geophysical Research Letters 22, 3091–3094.

Molchanov, O.A., Kulchitsky, A., Hayakawa, M., 2001. Inductive seismo-electromagnetic effect in relation to seismogenic ULF emission. Natural Hazards and Earth System Sciences 1, 61–67.

Morgunov, V., Matveyev, V., 1991. Electric and electromagnetic effects in the epicentral zone of Spitak aftershocks. Izvestija Earth Physics 27, 1002–1005.

Nagata, T., 1972. Application of tectonomagnetism to earthquake phenomena. Tectonophysics 14 (3/4), 263–271.

Nikiforova, N.N., Yadakhin, T.N., 1989. Studies of electromagnetic emission of tectonic origin in the Kirghiz SSR. Physics of the Earth and Planetary Interiors 57, 68–74.

Nitsan, U., 1977. Electromagnetic emission accompanying fracture of quartz-bearing rocks. Geophysical Research Letters 4/8, 333–335.

Obermeyer, H., 2005. Measurement of Natural Pulsed Electromagnetic Radiation (EMR) with the Cerescope. Ceres GmbH, Staffort.

O'Keefe, S.G., Thiel, S.V., 1995. A mechanism for the production of electromagnetic radiation during fracture of brittle materials. Physics of the Earth and Planetary Interiors 89, 127–135.

Rabinovitch, A., Bahat, D., Frid, V., 1996. Emission of electromagnetic radiation by rock fracturing. Zeitschrift für Geologische Wissenschaften 24 (3/4), 361–368.

Rabinovitch, A., Frid, V., Bahat, D., Goldbaum, J., 2000. Fracture area calculation from electromagnetic radiation and its use in chalk failure analysis. International Journal of Rock Mechanics and Mining Sciences 37, 1149–1154.

Reuther, C., Obermeyer, H., Reicherter, K., Reiss, S., Kaiser, A., Buchmann, T., Adam, J., Lohrmann, J., Grasso, M., 2002. Neotektonik und aktive Krustenspannungen in Südost-Sizilien und ihre Beziehungen zur regionalen Tektonik im Zentralen Mittelmeer. Mitteilungen aus dem Geologisch-Paläontologischen Institut der Universität Hamburg 86, 1–24.

Schmitt, T.J., 1981. The West European stress field: new data and interpretation. Journal of Structural Geology 3/3, 309–315.

Slifkin, L., 1993. Seismic electric signals from displacement of charged dislocations. Tectonophysics 224, 149–152.

Strobach, K., 1974. Model of crustal stresses in the region of the Rhinegraben in southwestern Germany. In: Illies, H., Fuchs, K. (Eds.), Approaches to Taphrogenesis. Int. Union Commiss. on Geodynamics Sci. Rep. 8, pp. 389–394.

Teisseyre, R., 1992. Earthquake premonitory processes: evolution of stresses and electric current generation. Terra Nova 4, 509–513.